The synthetic artificial stem cell (SASC): Shifting the paradigm of cell therapy in regenerative engineering

Shiv Shah[a,b,c], Caldon Jayson Esdaille[a,b], Maumita Bhattacharjee[a,b], Ho-Man Kan[a,b], and Cato T. Laurencin[a,b,c,d,e,f,g,h,1]

[a]Connecticut Convergence Institute for Translation in Regenerative Engineering, University of Connecticut Health Center, Farmington, CT 06030; [b]Raymond and Beverly Sackler Center for Biomedical, Biological, Physical and Engineering Sciences, University of Connecticut Health, Farmington, CT 06030; [c]Department of Chemical and Biomolecular Engineering, University of Connecticut, Storrs, CT 06269; [d]Department of Orthopedic Surgery, University of Connecticut Health, Farmington, CT 06030; [e]Department of Biomedical Engineering, University of Connecticut, Storrs, CT 06269; [f]Department of Materials Science and Engineering, University of Connecticut, Storrs, CT 06269; [g]Institute of Materials Science, University of Connecticut, Storrs, CT 06269; and [h]Department of Craniofacial Sciences, School of Dental Medicine, University of Connecticut Health, Farmington, CT 06030

Contributed by Cato T. Laurencin; received September 13, 2021; accepted November 22, 2021; reviewed by Guillermo Ameer and Jennifer Elisseeff

Stem cells are of great interest in tissue regeneration due to their ability to modulate the local microenvironment by secreting bioactive factors (collectively, secretome). However, secretome delivery through conditioned media still requires time-consuming cell isolation and maintenance and also may contain factors antagonistic to targeted tissue regeneration. We have therefore engineered a synthetic artificial stem cell (SASC) system which mimics the paracrine effect of the stem cell secretome and provides tailorability of the composition for targeted tissue regeneration. We report the first of many applications of the SASC system we have formulated to treat osteoarthritis (OA). Choosing growth factors important to chondrogenesis and encapsulating respective recombinant proteins in poly (lactic-coglycolic acid) 85:15 (PLGA) we fabricated the SASC system. We compared the antiinflammatory and chondroprotective effects of SASC to that of adipose-derived stem cells (ADSCs) using in vitro interleukin 1B-induced and in vivo collagenase-induced osteoarthritis rodent models. We have designed SASC as an injectable therapy with controlled release of the formulated secretome. In vitro, SASC showed significant antiinflammatory and chondroprotective effects as seen by the up-regulation of SOX9 and reduction of nitric oxide, ADAMTS5, and PRG4 genes compared to ADSCs. In vivo, treatment with SASC and ADSCs significantly attenuated cartilage degeneration and improved the biomechanical properties of the articular cartilage in comparison to OA control. This SASC system demonstrates the feasibility of developing a completely synthetic, tailorable stem cell secretome which reinforces the possibility of developing a new therapeutic strategy that provides better control over targeted tissue engineering applications.

stem cell | secretome | synthetic matrix | polymer | regeneration

Stem cell science has become an essential component of regenerative engineering and has the potential to revolutionize healing outcomes once clinical translation is achieved (1). Regenerative engineering utilizes a transdisciplinary approach and is defined by the convergence of advanced material science, stem cell sciences, physics, developmental biology, and clinical translation to regenerative complex tissues and organs (2, 3). Mesenchymal stem cells, which are a multipotent cell type, possess the ability to self-renew and differentiate into various lineages such as adipocytes, bone, cartilage, muscle, skin, and tendon and have been used in preclinical studies to regenerate these respective and other connective tissues (4, 5). In addition to their differentiation ability, stem cells also have the ability to secrete bioactive factors during differentiation which will further drive repair and regeneration (6, 7) As a result, the role of stem cells as progenitor cells with associated bioactive factors is becoming increasingly important as a strategy to harness the regenerative potential of the tissues within the body (8).

Stem cell therapy focuses on the delivery of cells to facilitate tissue repair and regeneration by a combination of antiinflammatory, immunomodulatory properties and multipotent differentiation capacity. However, in order to be used in a clinical setting, they must be isolated from human tissue and require constant growth and passage in in vitro culture environments. In addition, studies have reported that cells are at risk for undergoing spontaneous alterations in behavior and properties while being cultured (9). Contamination is also a risk due to improper technique or nonsterile conditions. Other limitations and challenges that should be considered when developing stem cell therapies include immune compatibility and rejection reactions, formation of malignant tumors due to uncontrolled proliferation, and transmission of infectious processes (10, 11).

Following these concerns and further reportedly negligible levels of stem cell engraftment into the diseased tissue (12), more recent studies are highlighting the fact that the collection of paracrine factors secreted by stem cells (known as the secretome) is the main enforcer of therapeutics effects. Cell-free alternatives that utilize paracrine factors in a similar fashion have recently been considered (13–16). Secretome has been proposed as a cell-free alternative to cell therapy to overcome

Significance

This paper presents the synthetic artificial stem cell (SASC) system: a versatile therapy which provides the ability to tailor paracrine responses of different cells and provide a more potent regenerative effect for targeted tissues. Upon challenging the SASC system against an osteoarthritis model, we demonstrate that the factors combined tailored for chondrogenesis have a potent antiinflammatory and chondroprotective effect. This paper also demonstrates the in vivo capacity of SASC to attenuate proteoglycan depletion in the cartilage extracellular matrix while also improving biomechanical properties of the resulting cartilage. We report the first of many applications of the SASC system, which provides a promising step toward clinical translation of a minimally immunogenic stem cell with many commercial advantages over its biological counterpart.

Author contributions: S.S. and C.T.L. designed research; S.S., C.J.E., M.B., and H.-M.K. performed research; S.S. contributed new reagents/analytic tools; S.S. and C.J.E. analyzed data; and S.S., C.J.E., M.B., H.-M.K., and C.T.L. wrote the paper.

Reviewers: G.A., Northwestern University; and J.E., Johns Hopkins University.

Competing interest statement: University of Connecticut has filed a patent application on behalf of the inventors (S.S., H.-M.K., and C.T.L.) entitled "The Synthetic Artificial Stem Cell." C.T.L. has the following competing financial interests: Mimedx and Biobind Soft Tissue Regeneration/Biorez.

[1]To whom correspondence may be addressed. Email: laurencin@uchc.edu.

This article contains supporting information online at http://www.pnas.org/lookup/suppl/doi:10.1073/pnas.2116865118/-/DCSupplemental.

Published January 5, 2022.

the limitations and associated risks with stem cell therapeutics. The secretome is defined as a set of biological factors and molecules that are secreted into the extracellular matrix (ECM) which play an essential role in a wide range of biological processes, including homeostasis, immunomodulation, inflammation, angiogenesis, and ECM organization (17). The functions of the secretome can be broken into four main functions: angiogenesis, antiapoptosis, antifibrosis, and antiinflammation (17). Various secreted proteins make up the cell secretome and can include growth factors, angiogenic factors, cytokines, chemokines, and extracellular vesicles for transport of lipids and proteins. The composition of the secretome is highly dynamic and is based on the cell type and microenvironment which it will be used in, allowing for greater design flexibility and versatility for use in a wide array of tissues (17, 18). The paracrine effect exhibited by the secretome has been shown to be very effective in regenerating different tissues (12) with several logistical advantages for use in a clinical setting such as longer shelf lives, availability, and scalability (19, 20).

While the secretome provides many advantages over cell-based therapy, it shares many similar translational challenges, including time-consuming cell maintenance to obtain conditioned media and compositional sensitivity to the cell microenvironment. Stem cells secrete a mixture of biological factors in a controlled, sequential, and combinatorial fashion to exhibit the paracrine effect which has recently been shown to be a key driver for the regenerative process. To date, there has been no study conducted which attempts to mimic the paracrine functions of the stem cell. While single growth factor treatment may not be effective for complete regeneration, controlled delivery of a mixture of factors is needed to truly mimic cellular paracrine functions. Therefore, we have engineered the synthetic artificial stem cell (SASC). With the added ability to tailor the formulation for targeted tissues, SASC has the potential to be used in different systems by providing potent immunomodulatory and regenerative effects.

In the present study, we aimed at developing the first SASC system to attenuate osteoarthritis (OA) progression by tailoring factors abundant in the stromal stem cell secretome that have specifically an anabolic, chondroprotective, and/or antiinflammatory effect in the joint (21–23). Katagiri et al. (23) found insulin-like growth factor (IGF) and transforming growth factor (TGF)-β1 to be important chondrogenic factors in bone marrow–derived stem cell conditioned media. Others have also reported the importance of fibroblast growth factor (FGF)-18 in chondrogenesis (specifically signaling through anabolic receptor FGFR3) (24–26) and of human growth hormone (HGH) (a proliferative factor which also signals for IGF1) (27, 28). As a pilot SASC composition, IGF1, TGF-β1, FGF-18, and HGH were combined at concentrations similar to conditioned media and delivered using a poly (lactic-coglycolic acid) (PLGA) 85:15 matrix. The antiinflammatory and chondroprotective effects of SASC have been evaluated in comparison with the current treatment standard, adipose-derived stem cells (ADSCs) (5), in both in vitro and in vivo OA models (Fig. 1). Furthermore, biomechanical outcomes of SASC treatment were also evaluated in vivo.

Results

Fabrication and Characterization of the SASC System. Growth factors, FGF-18, IGF1, HGH, and TGF-β1, were loaded individually into the PLGA matrix (10 ng growth factor/mg PLGA) using a modified double-emulsion method (29, 30). Scanning electron microscopy (SEM) was used to visualize microspheres that were in the 10- to 20-μm range as collected by sieving; 1,000× magnification was used to see shape and size while 10,000× magnification was used to see surface smoothness of each microsphere batch (Fig. 2). Microspheres of all batches, irrespective of growth factor loaded, maintained a smooth surface and similar size distribution while shrinking and surface wrinkling observed in the higher magnification images was an artifact of the electron beam. Loading efficiency of IGF1 was 88.95 ± 9.66% (Table 1). Release was observed separated into three phases: an initial burst with 30% surface loaded protein released within 1 d, a diffusion-controlled phase over the next 10 d, and finally an equilibrium-controlled release until 90% was released by the 28th day (Fig. 3*A*). The loading efficiency of HGH and TGF-β1 was found to be low due the large size, and hence bovine serum albumin (BSA) was used as a carrier protein to enhance the respective loading efficiencies. HGH with 1% BSA achieved 69.42 ± 12.48% loading (Table 1). Fifty percent of the loaded HGH was released over the first day and plateaued at this level for the remainder of the 28-d release period (Fig. 3*B*). TGF-β1 was loaded at 40.68 ± 4.04% efficiency with 3% BSA used (Table 1). The release of this large, hydrophobic molecule showed minimal burst and a much slower, linear release profile in which about 50% was released over 28 d (Fig. 3*C*).

Investigating the Antiinflammatory and Chondroprotective Effects of SASC. We used a coculture system as an indirect in vitro OA model (Fig. 1*A*). We used healthy chondrocytes and chondrocytes treated with a proinflammatory cytokine interleukin (IL)-1β (a prominent inflammatory marker produced during early stages of OA) as respective sham and negative treatment controls. The remaining cells were divided into three groups: inflamed chondrocytes treated with ADSCs, inflamed chondrocytes treated with blank (phosphate-buffered saline [PBS]-loaded particles), and inflamed chondrocytes treated with SASC. The approximate dose of each growth factor in the SASC group was 920 pg HGH and FGF-18, 1,186 pg IGF1, and 550 pg TGF-β1.

Nitric oxide assay evaluating the antiinflammatory property of SASC. Nitric oxide (NO) is expressed in the chondrocyte inflammatory process. An in vitro coculture system of chondrocytes and ADSCs was used to investigate the production of NO. Chondrocytes upon treatment with IL-1β showed significant increase in NO production that indicates inflammation in chondrocytes. The addition of ADSCs and the blank group did not reduce NO production of inflamed chondrocytes. However, the addition of SASC showed significantly lower production of NO, indicating the antiinflammatory property of SASC (Fig. 4*A*).

Gene expression analysis evaluating the antiinflammatory and chondroprotective effect. To investigate the inhibition of catabolic responses of IL-1β by SASC, quantitative real-time PCR (qRT-PCR) was performed to determine the gene expression of early chondrogenic transcription factor SOX9, matrix-degrading enzyme, a disintegrin and metalloproteinase with thrombospondin motifs 5 (ADAMTS5), as well as antiinflammatory factor proteoglycan 4 (PRG4), also known as lubricin. The IL-1β–treated group showed significant up-regulation of ADAMTS5 (Fig. 4*C*), while a significant down-regulation was observed for SOX9 (Fig. 4*B*) and PRG4 (Fig. 4*D*) compared to healthy chondrocytes. ADSCs were found to only attenuate the increased messenger RNA (mRNA) level of ADAMTS5 over the 3-d treatment period. SASC showed significant up-regulation of SOX9 and attenuation of increased NO, PRG4, and mRNA level of ADAMTS5 (Fig. 4 *B–D*), indicating the significant antiinflammatory and chondroprotective effect of SASC and versatility of an SASC treatment compared to ADSCs.

Evaluating In Vivo Cartilage Regeneration Potential of SASC. The potential of SASC to attenuate enzyme-induced articular cartilage degeneration was evaluated using an in vivo rodent model (31) (Fig. 1*B*) with the contralateral knee taken as a healthy control. After OA induction, we divided the animals into four treatment groups ($n = 11$): OA control treated with saline, rats

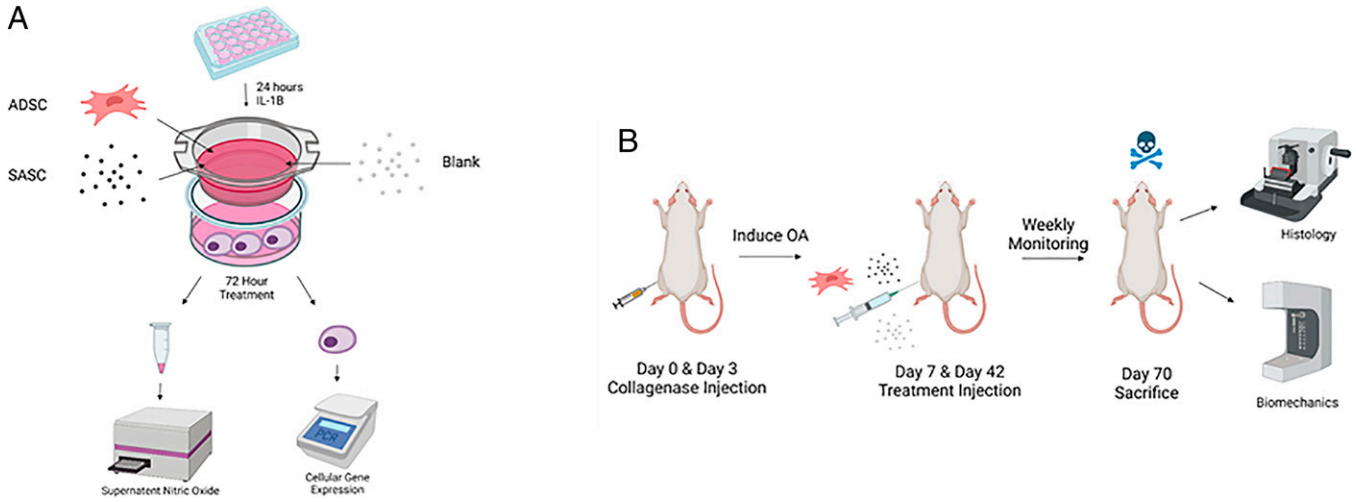

Fig. 1. A graphical summary of coculture in vitro (*A*) and rodent collagenase-induced in vivo (*B*) models. Figure made in Biorender.

injected with 1 million ADSCs suspended in saline, rats injected with 1 million blank particles in saline, and rats injected with 1 million SASC particles suspended in saline. The approximate dose of each growth factor in this group was 9.256 ng HGH and FGF-18, 11.86 ng IGF1, and 5.424 ng TGF-β1.

Joint swelling. Progression of inflammation, as indicated by gross swelling (Fig. 5), was slowed upon the first treatment of ADSC and the SASC. Following the initial treatment injection, joint swelling for the OA control progressed significantly at day 28, 1 wk before the second injection. While injection of the blank microspheres did have any effect on swelling, joint swelling in the ADSC- and SASC-injected joints was significantly lower than that of the OA group. Interestingly, 1 wk after the second treatment injection (day 42), the extent of swelling increased in all groups (Fig. 5). While the SASC-injected group continued to have lower swelling compared to the OA and blank groups, there was a continued progression of swelling between the second treatment injection and the end of the study. Two weeks after the second injection, swelling in both ADSC and OA group was similar; however, during the last 2 wk of the study the swelling in ADSC group significantly dropped to a level similar to SASC group.

Investigating effect on OA attenuation by safranin O staining. Frontal sections taken from the middle of the intact joint were stained with safranin O to assess the degenerated cartilage matrix area caused by the OA phenotype (Fig. 6). OA control animals showed loss of proteoglycan staining (Fig. 6*B*) as well as lesions and erosion at the articular surfaces (33.75 ± 7.81% total degenerated area). SASC- (Fig. 6*E*) and ADSC- (Fig. 6*C*) injected groups (10.03 ± 7.05% and 10.62 ± 7.33%, respectively) were comparable to the healthy joint (Fig. 6*A*) (7.53 ± 2.84%), showing strong safranin O staining which indicated the SASC

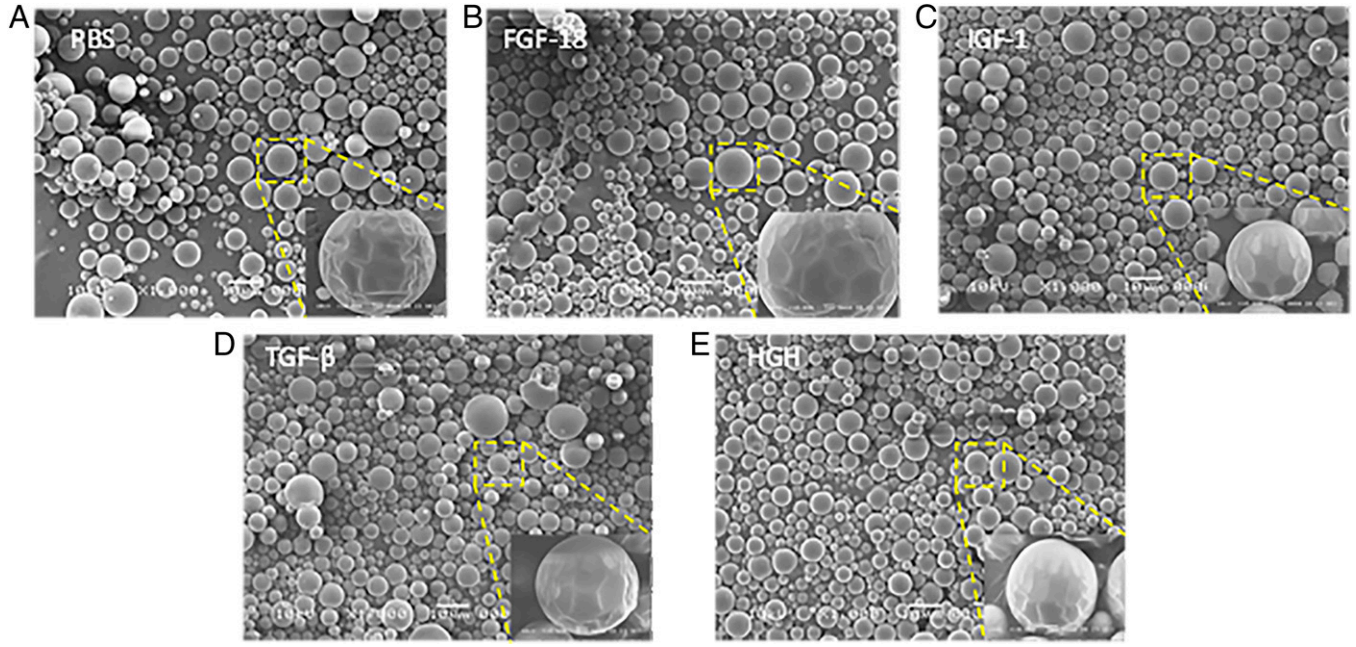

Fig. 2. SEM images of PLGA microspheres with PBS (*A*), microspheres loaded with FGF-18 (*B*), microspheres loaded with IGF1 (*C*), microspheres loaded with TGF-β1 (*D*), and microspheres loaded with HGH (*E*). Larger images were captured using 1,000× magnification (Scale bar, 10 μm), and smaller images in bottom right of each panel were captured under 10,000× magnification (Scale bar, 1 μm).

Table 1. Loading efficiency of IGF1, HGH, and TGF-β1 microspheres (n = 4)

Growth factor	% BSA needed	Loading efficiency
IGF1	0%	88.95 ± 9.66%
HGH	1%	69.42 ± 12.48%
TGF-β1	3%	40.68 ± 4.04%

Growth factors required different concentrations of carrier protein to achieve loading depending on their physical properties.

and ADSC treatments could significantly prevent loss of proteoglycan content of the cartilage ECM (Fig. 6*F*). Furthermore, treatment with the blank group (Fig. 6*D*) (30.61 ± 15.45%) did not have any effect in recovering the matrix, showing more prominent lesions and areas of erosion with no signs of cartilage matrix preservation. This confirmed the preservative effect of SASC was due to the controlled release of the synthetic secretome.

Evaluating biomechanical outcomes by nanoindentation. Heat maps produced for the average stiffness at each surface (Figs. 7 and 8) and statistical differences of the surface stiffness between groups were identified (Figs. 7*G* and 8*G*). OA cartilage had a significantly lower modulus (tibia: 0.96 ± 0.53 MPa; femur: 1.70 ± 0.74 Mpa) compared to the contralateral joint (tibia: 1.79 ± 0.61 Mpa; femur: 3.61 ± 1.56 Mpa) taken as a healthy control (Figs. 7 *A* and *B* and 8 *A* and *B*). Treatment with ADSC (tibia: 1.36 ± 0.66 Mpa; femur: 3.00 ± 1.88 Mpa) and SASC (Figs. 7 *C* and *E* and 8 *C* and *E*) (tibia: 1.41 ± 0.79 Mpa; femur: 2.35 ± 1.37 Mpa) resulted in an increased modulus, indicating recovery of cartilage stiffness, though this recovery was not similar to the healthy control using either treatment. Finally, the blank group (Figs. 7*D* and 8*D*) (tibia: 1.05 ± 0.61 Mpa; femur: 1.68 ± 0.62 Mpa) did not have any significant impact on the Young's modulus on either surface.

Discussion

Stem cells have been widely used in regenerative engineering due to their multipotent ability as well as their capability to produce paracrine factors that affect the local microenvironment. However, sensitivity to changes in the local microenvironment may lead to spontaneous changes in cellular function and the secreted factor composition, leading to challenges in translatability. In this study, we have engineered a completely synthetic, tailored alternative to the stem cell by loading certain factors found in the stem cell secretome into a PLGA matrix. As a pilot system, we formulated and evaluated the SASC system to attenuate OA. Herein, IGF1, TGF-β1, HGH, and FGF-18 were chosen for developing the SASC system.

It has been reported that IGF1 has anabolic and antiinflammatory effects on cartilage and chondrocytes and has been shown to stimulate proteoglycan and collagen synthesis as well as decrease rates of matrix degradation (32, 33). TGF-β1 has a variety of functions in articular cartilage development and maintenance of integrity. It has been shown to also stimulate ECM synthesis through chondrocyte differentiation and inhibition of hypertrophy and decrease matrix catabolism by attenuating activity of various matrix metalloproteases (MMPs) that may result in inflammation (34). In one study, sequential release of low doses of TGF-β1 also had an additive effect with IGF1 in promoting cartilage regeneration in similar PLGA-based scaffolds (35). HGH coordinates a variety of anabolic and catabolic reactions through JAK-STAT, ERK, P13K-Akt pathways and signaling has been used as a proliferative factor, stimulating native stem cell proliferation as well as signaling for IGF1 providing an indirect anabolic effect (27, 28). FGF-18, by selectively binding to FGFR3, has been shown to stimulate ECM in injured chondrocytes and increase native chondrocyte proliferation and chondrogenesis (24–26).

All of these growth factors were loaded using a standardized double emulsion (W/O/W) method with similar microsphere yields in the average size of a mesenchymal stem cell (10 to 20 μm) (36) (Fig. 2) (about 70%). Having a standardized fabrication method in which yield is not dependent on the factor being loaded proves greatly advantageous when looking at the versatility of SASC in which different growth factors may be used for different applications. We have successfully used one standardized process to load different factors while maintaining microsphere size, which minimizes optimization needed to load individual growth factors into microspheres.

We found IGF1 (about 7 kDa) had a high loading efficiency into these microspheres without the need for a carrier protein and also released almost completely from the microspheres within 28 d. The bigger HGH and TGF-β1 molecules, having about 20 and 40 kDa, respectively, required the use of a carrier protein (BSA) to be loaded into the microspheres, and while 60% of each factor released from the PLGA microspheres the profile of TGF-β1 was much more linear compared to the burst and subsequent plateau of HGH release, indicating that the larger size and slightly more hydrophobic nature of TGF-β1

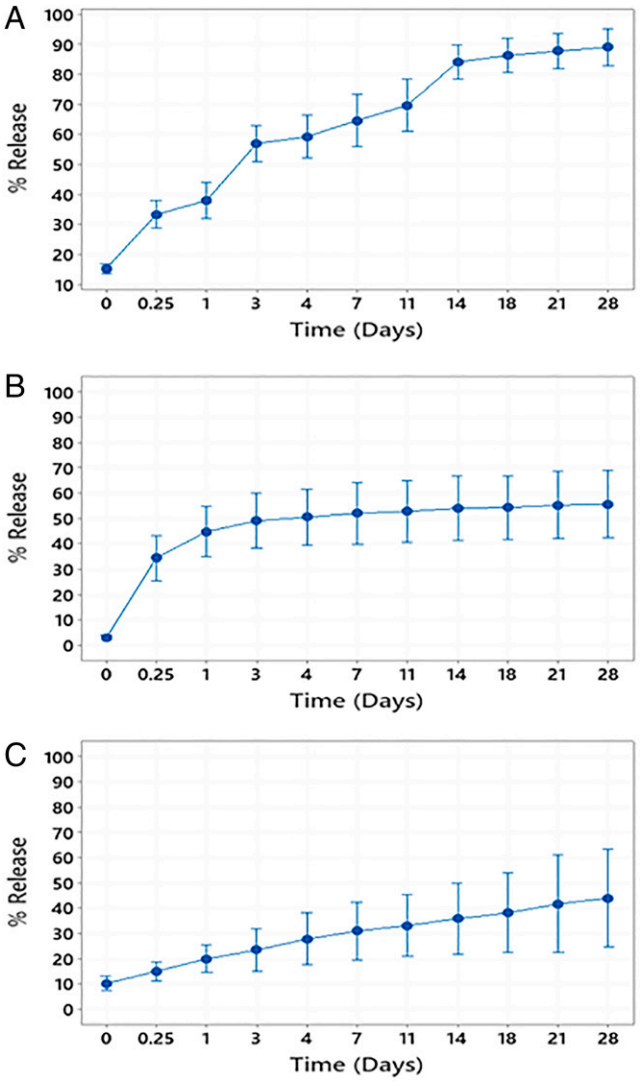

Fig. 3. Cumulative release profiles of IGF1 (*A*), HGH (*B*), and TGF-β1 (*C*) PLGA 85:15 microspheres. n = 4 batches measured in triplicate.

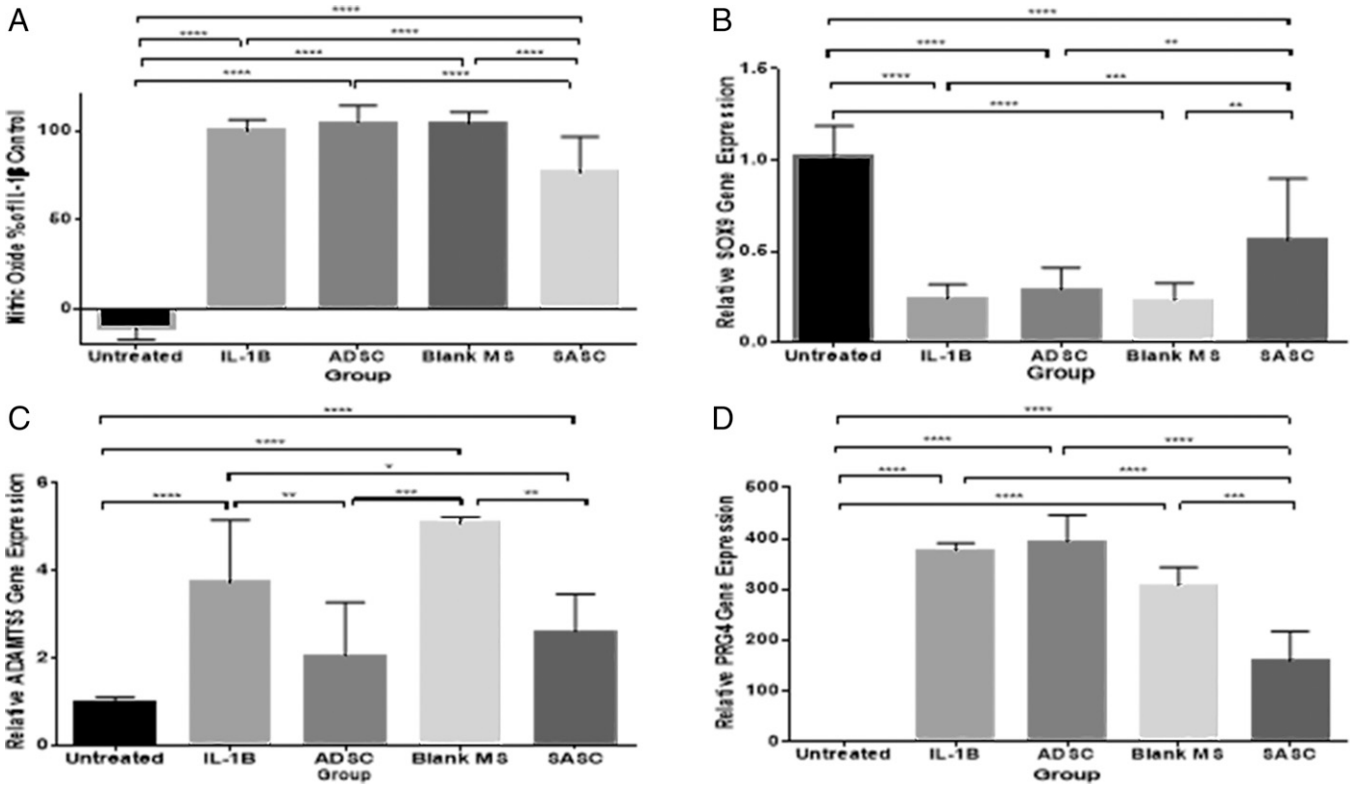

Fig. 4. SASC exhibits antiinflammatory and chondroprotective effects similar to ADSC. SASC reduced NO by Griess reagent assay (*A*), increased early chondrogenic marker SOX9 (*B*), and reduced catabolic gene expression of ADSMTS5 (*C*). SASC also reduced the autocrine inflammatory response of PRG4 (*D*). ADSCs were able to attenuate ADAMTS5 inflammatory response but did not have any effect on SOX9 or PRG4 or NO in the 3-d treatment window. **P* < 0.05; ***P* < 0.01; ****P* < 0.001; *****P* < 0.0001. Complete statistical summary provided in *SI Appendix*, Tables S1–S4.

may have played a role in hindering diffusion out of the microsphere. While all of these factors had different loading efficiencies, SEM images (Fig. 2) confirmed that microsphere physical characteristics were not affected and therefore loading efficiency could be a function of the biophysical properties of the factor being loaded. Because FGF-18 (about 20 kDa) has similar size to HGH we assumed that it would have similar loading properties and used the same amount of carrier protein.

In this study, we have used OA as a target model and engineered an SASC system consisting of growth factors that are able to stimulate ECM synthesis as well as reduce inflammation to disrupt the cycle of inflammation/degeneration. In the osteoarthritic joint, the homeostasis has been shifted toward catabolic processes, with the presence of M1 macrophages in the synovium stimulated by proinflammatory cytokines such as IL-1β and tumor necrosis factor alpha (37, 38). This stimulation perpetuates inflammation of the synovial membrane through the synthesis of inflammatory mediators such as matrix-degrading enzymes like ADAMTS5 and various MMPs. These enzymes then diffuse through the synovial fluid into the cartilage and start a vicious cycle of inflammation and degeneration characterized by chondrocyte hypertrophy and hypocellularity (38, 39).

In vitro characterization has shown that SASC is able to inhibit catabolic processes as a result of inflammation in chondrocytes. In our in vitro study, we have induced inflammation in rat chondrocytes with IL-1β which bears a close resemblance to the inflammatory process of the cartilage during OA (40). The paracrine effects of ADSC to those of SASC were compared in a coculture transwell system (Fig. 1*A*). NO is an inflammatory product generated through the inducible NOS (iNOS) pathway, which inhibits the synthesis of collagen and proteoglycans and increases activity of proteolytic enzymes. NO production in the IL-1β group increased with 20 ng/mL of IL-1β. Treatment with SASC particles for 3 d significantly decreased NO production (Fig. 4*A*), which can potentially be attributed to the suppression of the iNOS pathway with released TGF-β1 (41). Generally arthritic chondrocytes are less responsive to IGF1 because of the presence of iNOS (42). We believe, in our system, TGF-β1 reduced the expression of iNOS which further enhanced the chondrocyte response to anabolic IGF1, resulting in suppression of downstream inflammatory pathways. This led to a more potent antiinflammatory effect of SASC compared to the paracrine factors produced by ADSCs, which may also include a wide variety of iNOS-inducing factors (such as vascular endothelial growth factor).

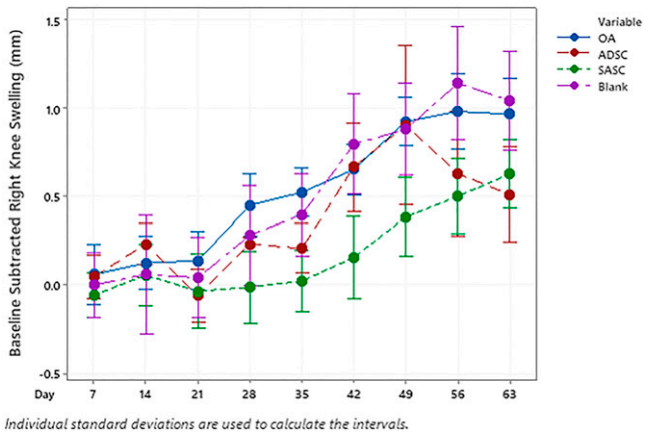

Fig. 5. Progression of ipsilateral joint inflammation over the 9-wk treatment period. Asterisk indicates the initial point when ADSC and SASC exhibit lower swelling compared to blank and OA groups.

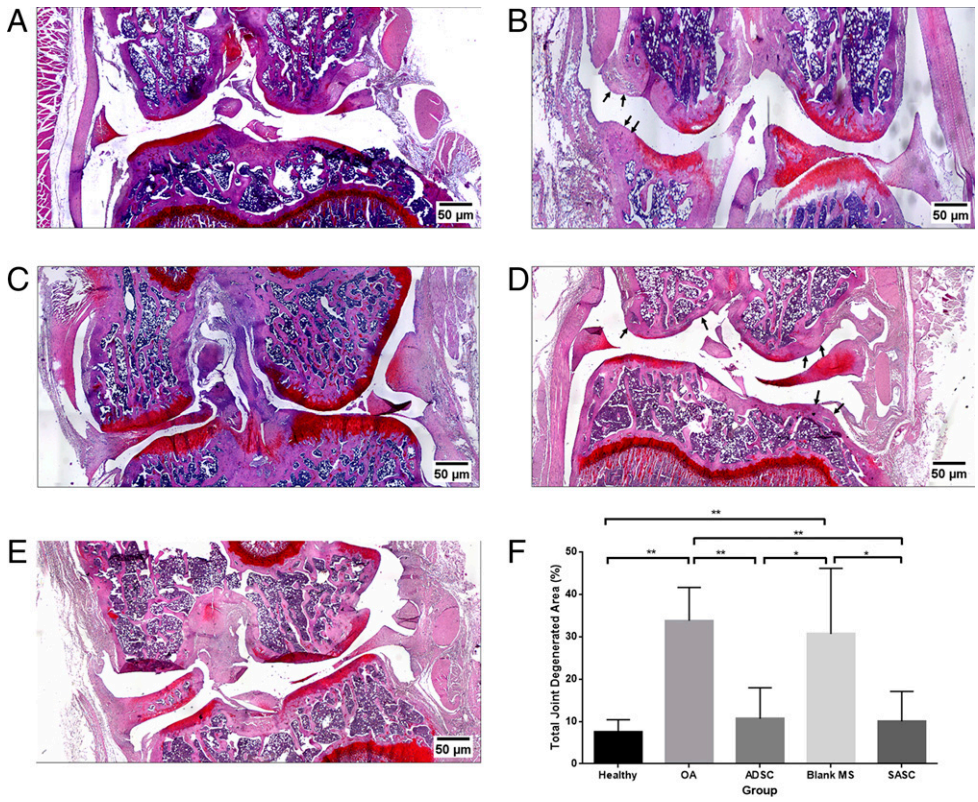

Fig. 6. Frontal sections of the healthy control (*A*), OA control (*B*), ADSC group (*C*), blank group (*D*), and SASC group (*E*). Quantification of degenerated areas shows SASC and ADSC attenuate progression of degenerative OA (*F*). Arrows point to areas of significant cartilage thinning/degeneration. $*P < 0.05$; $**P < 0.01$. $n = 5$. Complete statistical summary provided in *SI Appendix*, Table S5.

As an effect of IL-1β inflammation induction, expression of the master chondrogenic transcription factor SOX9 was down-regulated and aggrecanase ADAMTS5 was increased. SOX9 signals for early chondrogenesis, leading to the production of ECM proteoglycans such as collagen II and aggrecan. The down-regulation of SOX9 by IL-1β indicates a loss of early chondrocytes and indicates hypocellularity could occur. SASC's potent up-regulation of SOX9 (Fig. 4*B*) may be attributed to the presence of high IGF1 and FGF-18, factors important to chondrocyte proliferation and ECM production (24–26, 33, 42). Lubricin or PRG4 serves as both a boundary lubricant and a chondroprotective agent (43). Previous reports have shown decreased lubricin concentration in anterior cruciate ligament transection-induced OA in rodents and humans as well as in humans with late-stage chronic OA. On the contrary, there are studies conducted in sheep, dogs, and horses that have observed an increase of PRG4 in OA models, emphasizing the complex and sensitive autocrine role PRG4 plays in modulating progression of OA (43–48). An increase in PRG4 upon IL-1β–induced inflammation was observed and may indicate a negative feedback regulation of inflammation. Interestingly, in addition to having a similar antiinflammatory effect compared to ADSCs [reducing inflammatory effects ADAMTS5 (49, 50)], SASC was able to reverse the effects of inflammation on NO, SOX9, and PRG4 (Fig. 4 *A–D*). Therefore, SASC is shown to contribute a more potent chondroprotective effect as a result of the targeted composition of growth factors used in this composition.

A collagenase induced OA model was used to evaluate the in vivo chondroprotective potential of SASC. This model has been established to investigate the mechanisms of OA pathogenesis (31). Collagenase digests the collagen directly from cartilage ECM, resulting in similar osteoarthritic changes such as pain, changes in synovial membrane, subchondral bone remodeling, and degeneration of articular cartilage.

The dose of each growth factor in SASC was determined according to previous studies. Katagiri et al. found the composition of bone marrow stem cell conditioned media contained 1,368 ± 465 pg/mL IGF1 and 339.8 ± 14.4 pg/mL TGF-β1 (21–23). Other groups have used higher doses of IGF1 in treatment of OA ranging from 5 to 100 ng in rabbit models and as high as 100 μg weekly injections in a rat models (51–53). HGH analogs have been used to successfully treat cartilage defects in doses of 25 to 250 μg (54, 55) and FGF-18 in doses of 0.1 to 5 μg (26, 56) in rabbit models.

We elected to use lower doses of HGH and FGF-18 (9.256 ng each) to adjust for the difference in average size between the rabbit models referenced and the rat models used in this study. We have used IGF1 and TGF-β1 doses (11.86 ng and 5.424 ng, respectively) similar to those calculated from the respective conditioned media concentrations found by Katagiri et al (22, 23). We also added blank microspheres in this composition to simulate the possibility of adding or removing factors that might be necessary for better tailoring therapeutic outcomes for different tissues. In this case, we determined that equal weight fractions of growth factor loaded spheres (20% wt/wt for each) could be combined to deliver the calculated doses in vivo.

Previous studies have demonstrated the advantages and positive outcomes of combining one or two factors (35, 57) in chondrogenesis, though to date there have been no studies conducted to develop a mimic for the paracrine effect of a stem cell. Additionally, by harnessing different factor release patterns and loading efficiencies SASC can be formulated using different weight ratios and tailored to become a unique synthetic cell therapy for other degenerative diseases or regenerative applications.

Joint swelling is one of the most prominent symptoms of OA. It is usually indicative of synovitis, as the synovium within

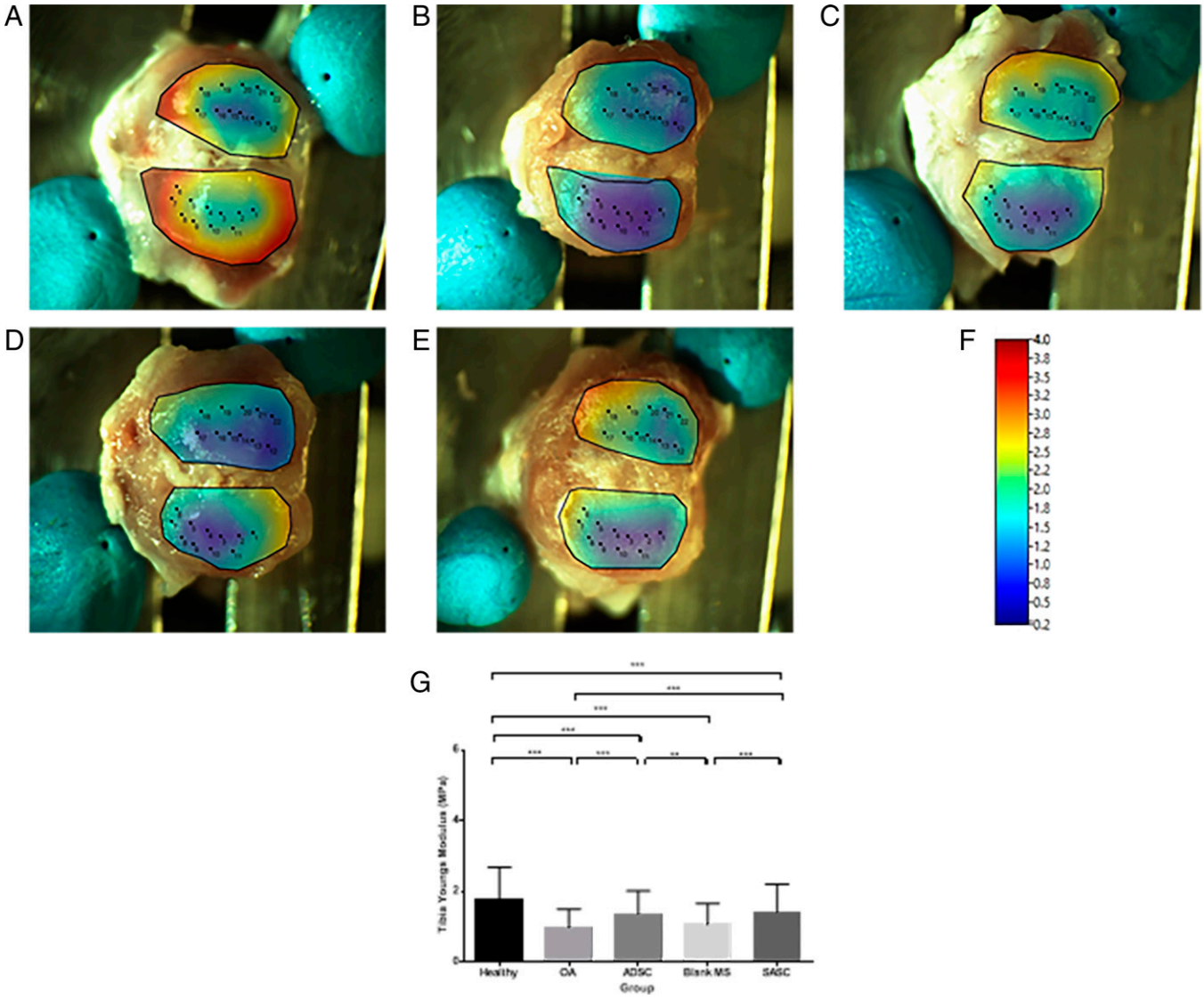

Fig. 7. Surface heat map depicting tibial Young's modulus (megapascals) of healthy (*A*), OA (*B*), ADSC- (*C*), blank- (*D*), and SASC- (*E*) treated joints (scale in *F*) and comparison of tibial Young's modulus across groups (*G*). $^{**}P < 0.01$; $^{***}P < 0.0001$. Complete statistical summary provided in *SI Appendix*, Table S6.

the joint may accumulate a number of inflammatory mediators which may contribute to the pain and further cartilage degeneration during OA (58).

Although the inflammatory response to blank particles was similar to the OA group as seen in Figs. 5 and 6, we believe that this response is mediated by collagenase and not the PLGA matrix. The clinical use of PLGA as a biocompatible vehicle for sustained release of therapeutics has been thoroughly investigated in prior studies. Zhang and Huang observed injection of PLGA microspheres induced a mild inflammatory response 1 d postinjection which subsided after 1 wk (59). Other clinical trials have also indicated that PLGA microspheres do not induce any deleterious effects on cartilage or any aspects of joint structure over a period of 24 wk (60). Therefore we do not expect that PLGA blank microspheres would evoke any additional inflammatory response. In addition, studies have shown the inflammatory response is size-dependent to micro/nano particles, demonstrating that smaller molecules (<5 μm in diameter) are extensively phagocytosed by macrophages in the epithelial synovial lining which induce a higher inflammatory response in the synovial tissue (61–63). As our microspheres were in the 10- to 20-μm range (similar to the size of mesenchymal stem cells), we do not anticipate phagocytosis-mediated inflammation.

On day 28 after the first injection, ADSCs and SASC resulted in a significant decrease compared to OA and blank controls. A more pronounced swelling was observed 2 wk after the second treatment (at day 49) in both the treatment groups. Though the swelling in the ADSC group decreased after 49 d, swelling in the SASC group continued to increase incrementally (Fig. 5). This difference between ADSC and SASC was not significant and both remained significantly lower compared to the OA group by day 63. This response in the SASC group may be due to increased macrophage activity in response to increased polymer load in the joint, but whether these macrophages are proinflammatory M1 macrophages or antiinflammatory M2 macrophages (41) is yet to be determined. However, the decrease in cartilage degeneration (Fig. 6*F*) could be attributed to a shift toward higher M2 activity in the swollen joints.

SASC was also shown to attenuate degenerative OA to a similar extent as ADSCs in vivo. Safranin O staining used to visualize degenerated articular cartilage matrix showed little to no degeneration in harvested SASC and ADSC samples, similar to the

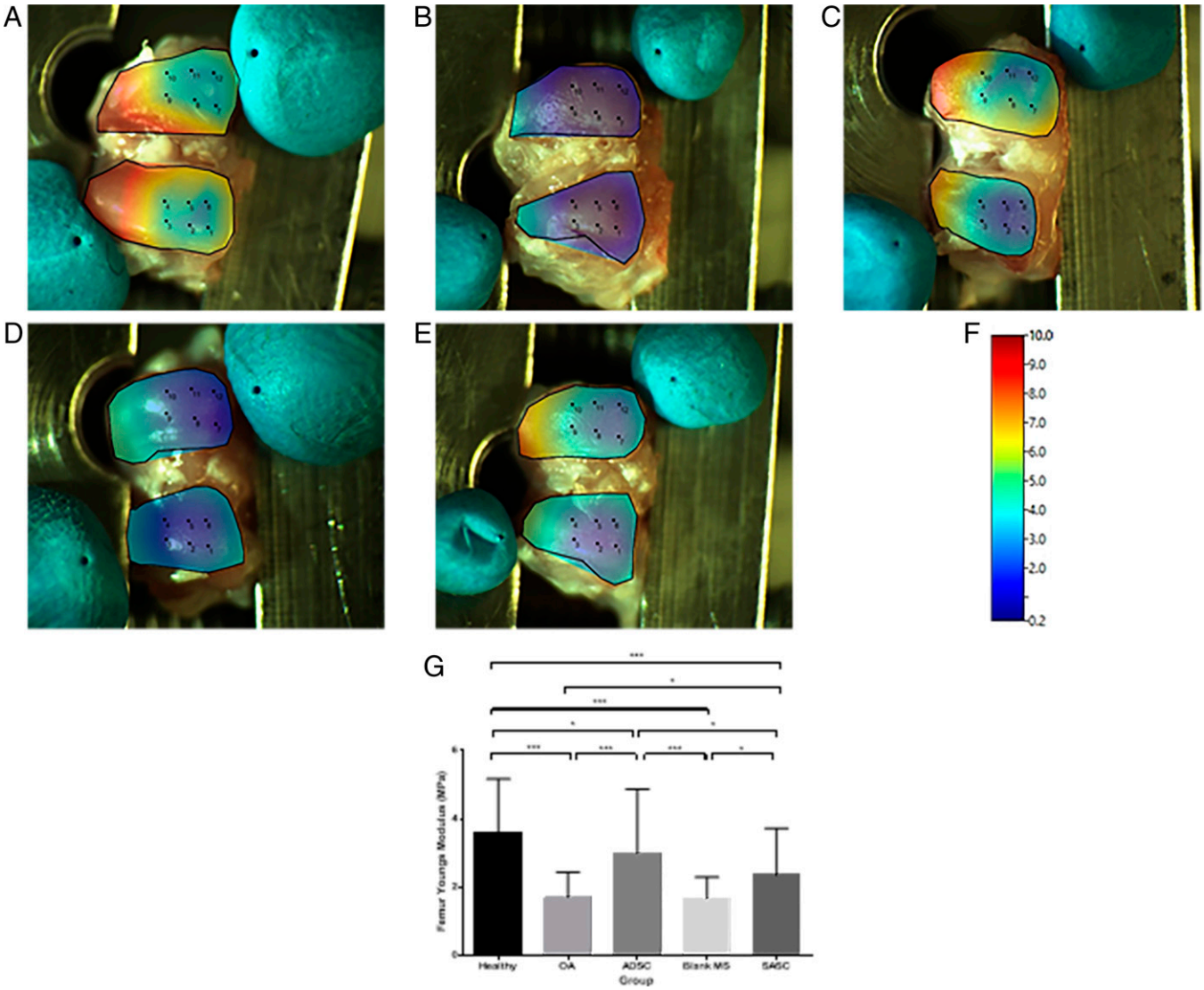

Fig. 8. Surface heat map depicting femoral Young's modulus (megapascals) of healthy (*A*), OA (*B*), ADSC- (*C*), blank- (*D*), and SASC- (*E*) treated joints (scale in *F*) and comparison of femoral Young's modulus across groups (*G*). $*P < 0.05$; $***P < 0.0001$. Complete statistical summary provided in *SI Appendix*, Table S7.

contralateral joints as healthy control. Nanoindentation on the surface of the cartilage was done to investigate whether the resulting cartilage was biomechanically superior to OA cartilage and similar to healthy articular cartilage. As a result of the degenerated cartilage solid network in OA, the stiffness of the cartilage (as measured by the Young's modulus) is decreased (64, 65). While PLGA microspheres with PBS did not recover the Young's modulus, ADSCs and SASC significantly increased the tibial and femoral modulus compared to OA (Figs. 7 and 8). However, neither modulus was similar to that of the healthy contralateral tibia or femur, indicating potential fibrillation of the cartilage that could be addressed in future SASC compositions.

In conclusion, our SASC system opens possibilities to tailor paracrine responses of different cells as well as provide a more potent regenerative effect for targeted tissues. Importantly, due to its small size, SASC is a minimally invasive, injectable therapy that can be injected in high particle concentrations as well as the ability to combine multiple growth factor-loaded microspheres in different weight ratios to tailor the composition in smaller injection volumes. Additionally, the synthetic nature of SASC mitigates risk associated with immunogenicity as well as variability in stem cell paracrine response due to donor properties. SASC is a synthetic system that uses a tailored mixture of biological factors designed to mimic the paracrine effect of a stem cell. These studies also suggest that SASC may be a clinically translatable stem cell substitute. In vitro, SASC exhibits antiinflammatory and chondroprotective effects similar to ADSCs on IL-1β–inflamed chondrocytes. In vivo, two treatments of SASC have successfully attenuated cartilage degeneration resulting from enzyme-induced OA, and this cartilage is mechanically superior to OA cartilage though still less stiff than healthy cartilage. This suggests that SASC can provide a comparable effect to the ADSCs. To better understand how SASC affects the local joint environment, a mechanistic investigation should be done along with identification of any potential systemic antiinflammatory responses and tracking the fate of SASC after injection.

Future Directions. The introduction of SASC shifts the paradigm of stem cell therapy into the synthetic domain. Loading of a recombinant secretome into a synthetic matrix provides a tailorable technology for many different areas of regenerative engineering. While the study in this paper focuses on the application of

SASC in attenuating OA progression, other systemic degenerative diseases may be evaluated. Furthermore, regeneration of various tissues requires different types of scaffolds, many of which stem cells are seeded to provide a biological cue to initiate regeneration. Combining SASC into such scaffolds would enhance retention in a local environment and provide these required cues exactly as seeded cells.

Materials and Methods

SASC Fabrication. Different microsphere batches for each growth factor were made using a modified double (w/o/w) emulsion solvent evaporation method (29, 30). Briefly, 250 mg of PLGA was dissolved in 4 mL of dichloromethane (DCM). A bulk aqueous solution of 1% (wt/vol) polyvinyl alcohol (PVA) + 1% (vol/vol) isopropyl alcohol (IPA) + 10% (wt/vol) NaCl was prepared. In a 250-mL beaker, 100 mL of 2% (vol/vol) IPA was added to 100 mL of a 2 (wt/vol) % PVA solution. NaCl was added to make a 10% wt/vol bulk solution. Growth factors were then diluted with PBS + 4% BSA to reach a final concentration of 1% BSA for HGH and FGF-18 and 3% for TGF-β1 and a final volume of 100 μL. The theoretical loading of each growth factor was 10 ng growth factor/mg PLGA. Blank microspheres were prepared using 100 μL of PBS.

After PLGA dissolution, the growth factor or blank solutions were emulsified by vortexing at maximum speed for 30 s. Immediately, 4 mL of 5% PVA was added to make the secondary emulsion and this was vortexed for another 30 s at maximum speed. The double emulsion was injected into the bulk solution through an 18-gauge needle. The solution was stirred at 600 rpm for 3 h to allow for DCM extraction and evaporation. After evaporation, microspheres were centrifuged at 2,000 rcf for 3 min, subsequently washed with 250 mL water three times by filtration and lyophilized overnight. Microspheres in the 10- to 20-μm size range were separated by sieving and stored at −20 °C with desiccant until combined to form the final SASC composition. The composition of SASC used for the following studies was 20% by weight FGF-18 microspheres, 20% by weight TGF-β1 microspheres, 20% by weight IGF1 microspheres, and 20% by weight HGH microspheres and remaining blank microspheres. The blank microspheres were added to this composition to allow for increases in weight composition to allow for addition of an additional factor if needed. SASC and blank microspheres were sterilized for 20 min.

Particle Size Distribution. Microspheres size distribution was determined by sieving. Mass fractions were determined by dividing the weight of microspheres in the respective size bucket by the total weight of microspheres determined by the sum in all sieves. Microspheres in the 10- to 20-μm range were separated and sterilized for 20 min. Sterilized microspheres were used for further in vitro and in vivo testing.

SEM. For each growth factor-loaded microsphere batch, sieved microspheres were mounted on carbon tape and sputter-coated (Denton Vacuum Desk V) at 20 mA for 60 s. SEM (JEOL JSM-5900LV) images were taken using 10-kV voltage and spot size 23; 1,000× magnification was used to see general shape and size distribution and 10,000× magnification to see surface smoothness and any porosity. As the electron beam at 10,000× magnification damaged the microsphere structure, brightness and contrast were adjusted on a single sphere and images were captured using an adjacent sphere.

Loading Efficiency. For each growth factor, 10-mg microspheres were dissolved in 2 mL DCM at 37 °C for 1 h ($n = 4$). PBS, 2 mL, was added and the solution was vortexed for 30 s to allow extraction of the growth factor followed by centrifugation at 2,000 rcf for 3 min for phase separation. The top layer was aspirated and replaced with fresh PBS to repeat the process two times for a final extract volume of 6 mL. Enzyme-linked immunosorbent assay (ELISA) was performed in triplicate to calculate the loading efficiency using 100 ng as the theoretical mass of growth factor loaded in 10-mg microspheres.

Control Release Study. Release profiles for each growth factor were made for 10-mg microspheres in 2 mL PBS ($n = 4$). At predetermined time points, samples were centrifuged for 1 min at 2,000 rcf and 1 mL of the medium was collected for ELISA and replaced by 1 mL fresh PBS. The sample was briefly vortexed for microsphere resuspension and placed back into the water bath. ELISA was performed in triplicate to calculate the released mass and percent release was calculated using the loading efficiency.

ADSC Isolation and Culture. ADSCs were isolated from 6- to 8-wk-old Sprague–Dawley rats in accordance with the experimental guidelines and regulations approved by University of Connecticut Health Center Institutional Animal Care and Use Committee–approved protocol. ADSCs were isolated and purified as described by Bhattacharjee et al. (49). Rats were killed with CO_2 asphyxiation followed by cervical dislocation. Killed rats were weighed, shaved, and cleaned with 70% ethanol. Inguinal fat pads were isolated and weighed. The fat pads were collected, washed in sterile Hank's balanced salt solution (HBSS) with 1% penicillin/streptomycin (pen/strep), and minced into small pieces. The pieces were added to 25 mL collagenase type I (300 U/mL) (Invitrogen) in HBSS and agitated at 37 °C for 90 min (49). The resulting cell suspension was filtered through a 70-μm filter (BD Bioscience) for the removal of the solid aggregates. An equal volume of DMEM-F12 with 10% fetal bovine serum (FBS) and 1% pen/strep was added to neutralize the collagenase. The mixture was centrifuged at 1,500 rpm for 10 min, the supernatant was discarded, and the pellet was resuspended in 2 mL of red cell lysis buffer and incubated for 2 min at 37 °C. The mixture was again centrifuged at 1,500 rpm for 10 min. The supernatant was discarded and cells were counted and plated in a T150 flask containing DMEM-F12 with 10% FBS and 1% pen/strep (49). The media was changed after 24 to 48 h to remove cell debris and nonadhering cells. Passage 0 (P0) ADSCs were cultured in T150 flasks for 2 wk, in DMEM-F12 supplemented with 1% pen/strep. ADSCs reaching 80 to 90% confluence were detached with 0.25% trypsin (Thermo Scientific) at 37 °C, centrifuged at 1,500 rpm for 10 min, and replated. ADSCs were characterized by flow cytometry using cell surface markers (Becton-Dickinson LSR II; BD Biosciences) at passage 3 (P3). Cells were washed using sterile PBS, centrifuged, and resuspended in sterile fluorescence-activated cell sorting (FACS) buffer (PBS, 1% FBS) containing 10 μL of the FITC-conjugated CD29 antibody, fluorescein isothiocyanate (FITC)-conjugated CD90 antibody, FITC-conjugated CD34, FITC-conjugated CD45, and PE-conjugated CD11b for 30 min. Unlabeled cells were used as controls (49). Cells were then scanned with FACS, acquired and gated using forward scatter (FSC) and side scatter (SSC) parameters to exclude cell debris and aggregates (see *SI Appendix*, Fig. S1).

Coculture. All incubation and culturing was done at 37 °C, 5% CO_2, and 85% relative humidity. Primary chondrocytes were passaged through P4 and then 100,000 cells were seeded into a 24-well plate for NO and PCR analysis. Media containing DMEM-F12, 10% FBS, and 1% pen/strep was used to passage and initially seeding the cells. After cell attachment, the media was changed to DMEM-F12, 5% FBS, and 1% pen/strep for the negative control and DMEM-F12, 5% FBS, 1% pen/strep, and 20 ng/mL IL-1β for all other groups. Cells were incubated for 24 h to allow induction of inflammation. After induction, 100,000 ADSCs, blank microspheres, or SASC were added into respective transwell inserts for coculture with inflamed chondrocytes. The media was also refreshed with fresh media (DMEM-F12 + 5% FBS + 1% pen/strep ± 20 ng/mL IL-1β).

The treatment went on for 72 h, after which the media was collected for NO analysis and frozen at −80 °C until analysis.

Griess Reagent Assay. NO concentration was measured using the Griess reagent assay. Standards were made by serial dilution of the stock in 5% DMEM-F12 + 5% FBS + 1% pen/strep. Standards and samples were then plates according to the manufacturer's procedures. The plate was incubated in for 30 min and the absorbance was read at 550 nm. A standard curve was made from blank subtracted standards and then NO content was calculated from the blank subtracted sample readings using the best-fit linear trend line.

qRT-PCR. qRT-PCR was done using a procedure used in our group (49). Briefly, total RNA was isolated from cells pooled from four wells using the RNeasy Mini Kit (74104; Qiagen) according to the manufacturer's instructions. For complementary DNA (cDNA) synthesis, 2 to 4 μg total RNA was used as a template for cDNA synthesis using EcoDry premix (639549; Takara) in a total volume of 20 μL (49). For qRT-PCR, iCycler Thermal Cycler Base (Bio-Rad) and iQ Supermix (Bio-Rad), SOX-9, ADAMTS5, PRG4, and GAPDH Taqman gene probes were used. The threshold cycle values of target genes were standardized against GAPDH expression and normalized to the expression in the untreated control culture. The fold change in expression of sample triplicates was calculated using the ΔΔCt comparative threshold cycle method (49).

Induction and Treatment of OA. This experimental protocol was approved by the Institutional Animal Care Committee, Uconn Health. Sprague-Dawley rats were acclimated for at least 24 h before procedure after being purchased from the vendor. On day 0 and day 3, animals were injected with 500 U of collagenase type II to induce an OA phenotype. Animals were then divided into four treatment groups ($n = 11$) injected on day 7: OA control treated with saline, rats injected with 1 million ADSCs suspended in saline, rats injected with 1 million SASC particles suspended in saline, and rats injected with 1 million blank microspheres in saline. A second treatment dose was given to all animals at 5 wk after first treatment. Using a hemacytometer, we determined that there were 150,000 spheres/mg and used this to determine the corresponding mass needed for 1 million microspheres (6.67 mg). For the SASC

group, the dose of each growth factor was then determined as 9.256 ng HGH and FGF-18, 11.86 ng IGF1, and 5.424 ng TGF-β1.

On each day of injection, rats were anesthetized with 2 to 4% isofluorane. The right knee was shaved and the diameter of both knees was measured by caliper. The right knee was prepped with Betadine and 70% ethanol and under fluoroscopic guidance, the respective solution was intraarticularly injected. The extent of knee swelling was monitored weekly until rats were killed at week 9.

Histology. Upon killing, knee joints were harvested and separated for histological and biomechanical evaluation. Contralateral joints were taken as a healthy control. Those joints taken for biomechanics were wrapped in PBS-dampened gauze, vacuum-sealed, and then stored at −20 °C until analysis. Joints used for histology were tied in a fully extended position on a cotton applicator stick and then fixed in 10% formalin for 5 to 7 d at 4 °C and then washed three times with PBS in 1-h storage intervals at 4 °C. Decalcification was done in Cal-EX for 3 d at 4 °C, changing the solution every day, followed by rinsing overnight with constantly running distilled water. Joints were then cut in half along the frontal plane and submitted to a core facility for processing and paraffin embedding. Five-micrometer sections were taken at about 350 μm into the block and stained with hematoxylin/eosin followed by a 15-min incubation in safranin O prior to dehydration. Articular surface areas of the femoral condyles and tibial plateaus (areas stained red with safranin O), measured between the ligament insertion site and the lateral or medial end of the bone, were identified and areas were quantified using ImageJ image analysis software. Areas of degeneration where there was no red staining by safranin O were measured using imageJ and the percent degeneration at the joint was measured using the following formula:

$$\%\ \text{Degeneration} = \frac{\sum \text{Degenerated Areas}}{\sum \text{Theoretical Healthy Articular Surface Area}} * 100.$$

Biomechanics. Joints were thawed in PBS with low agitation for at least 30 min. The joint was then dissected to expose the femoral and tibial articular cartilage. For the automated indentation of the articular cartilage, a 70-N multiaxial load cell with an amplification module was employed and calibrated prior to each use. The femurs and tibias in PBS were subjected to automated indentation at 12 and 22 predefined positions, respectively, using a 0.3-mm spherical tip indenter over each surface. Positions were evenly mapped on the lateral and medial sides of each bone. Automated indentation was done to a depth of 0.05 mm, at a speed of 0.05 mm/s with 10 s relaxation, as an initial scan and to ensure sufficient signal (load) was obtained with a 100-Hz data acquisition rate. Stress relaxation curves were observed with indentation of the articular cartilage. Structural stiffness was then calculated at an appropriate indentation depth and mapped at the indented positions.

Statistics. Minitab 19 was used to run an ANOVA with a two-sided 95% confidence interval for each in vitro comparison and degenerated area comparison. To analyze biomechanical differences between samples, a linear mixed effects model with two-sided 95% confidence interval was done in Minitab 19 to account for multiple measurement positions being combined to make up the whole cartilage surface stiffness. A Tukey's means comparison was done to evaluate intergroup differences. GraphPad Prism 6 was used to graph all figure data.

Data Availability. All study data are included in the article and/or *SI Appendix*.

ACKNOWLEDGMENTS. We thank the Center for Comparative Medicine and the central electron microscopy facility at University of Connecticut Health Center. We also thank the laboratory of Dr. Tannin Schmidt at University of Connecticut Health Center for lending use and training on their Biomomentum Mach 1 and Dr. Chia-Ling Kuo of the Connecticut Convergence Institute for Translation in Regenerative Engineering for her help with statistical analysis. This research was supported by NIH Grants DP1AR068147 and NIH T32 AR079114.

1. V. N. Vernekar, R. James, K. J. Smith, C. T. Laurencin, Nanotechnology applications in stem cell science for regenerative engineering. *J. Nanosci. Nanotechnol.* **16**, 8953–8965 (2016).
2. C. T. Laurencin, Y. Khan, *Regenerative Engineering: Advanced Materials Science Principles* (CRC Press, 2013).
3. C. T. Laurencin, Y. Khan, Regenerative engineering. *Sci. Transl. Med.* **4**, 160ed9 (2012).
4. A. I. Caplan, *Review:* Mesenchymal stem cells: Cell-based reconstructive therapy in orthopedics. *Tissue Eng.* **11**, 1198–1211 (2005).
5. S. Shah, T. Otsuka, M. Bhattacharjee, C. T. Laurencin, Minimally invasive cellular therapies for osteoarthritis treatment. *Regen. Eng. Transl. Med.* **7**, 76–90 (2020).
6. A. Naji *et al.*, Biological functions of mesenchymal stem cells and clinical implications. *Cell. Mol. Life Sci.* **76**, 3323–3348 (2019).
7. T. E. G. Krueger, D. L. J. Thorek, S. R. Denmeade, J. T. Isaacs, W. N. Brennen, Concise review: Mesenchymal stem cell-based drug delivery: The good, the bad, the ugly, and the promise. *Stem Cells Transl. Med.* **7**, 651–663 (2018).
8. G. Narayanan, M. Bhattacharjee, L. S. Nair, C. T. Laurencin, Musculoskeletal tissue regeneration: The role of the stem cells. *Regen. Eng. Transl. Med.* **3**, 133–165 (2017).
9. V. Turinetto, E. Vitale, C. Giachino, Senescence in human mesenchymal stem cells: Functional changes and implications in stem cell-based therapy. *Int. J. Mol. Sci.* **17**, 1164 (2016).
10. B. Lukomska *et al.*, Challenges and controversies in human mesenchymal stem cell therapy. *Stem Cells Int.* **2019**, 9628536 (2019).
11. C. T. Laurencin, A. McClinton, Regenerative cell-based therapies: Cutting edge, bleeding edge, and off the edge. *Regen. Eng. Transl. Med.* **6**, 78–89 (2020).
12. R. Mitchell *et al.*, Secretome of adipose-derived mesenchymal stem cells promotes skeletal muscle regeneration through synergistic action of extracellular vesicle cargo and soluble proteins. *Stem Cell Res. Ther.* **10**, 116 (2019).
13. G. Maguire, Stem cell therapy without the cells. *Commun. Integr. Biol.* **6**, e26631 (2013).
14. Y. Zhou, Y. Yamamoto, Z. Xiao, T. Ochiya, The immunomodulatory functions of mesenchymal stromal/stem cells mediated via paracrine activity. *J. Clin. Med.* **8**, 1025 (2019).
15. P. Menasché, Cell therapy trials for heart regeneration - Lessons learned and future directions. *Nat. Rev. Cardiol.* **15**, 659–671 (2018).
16. E. Eggenhofer, F. Luk, M. H. Dahlke, M. J. Hoogduijn, The life and fate of mesenchymal stem cells. *Front. Immunol.* **5**, 148 (2014).
17. L. Daneshmandi *et al.*, Emergence of the stem cell secretome in regenerative engineering. *Trends Biotechnol.* **38**, 1373–1384 (2020).
18. S. Eleuteri, A. Fierabracci, Insights into the secretome of mesenchymal stem cells and its potential applications. *Int. J. Mol. Sci.* **20**, 4597 (2019).
19. F. J. Vizoso, N. Eiro, S. Cid, J. Schneider, R. Perez-Fernandez, Mesenchymal stem cell secretome: Toward cell-free therapeutic strategies in regenerative medicine. *Int. J. Mol. Sci.* **18**, 1852 (2017).
20. P. Van Pham, H. T. Nguyen, N. B. Vu, "Evolution of stem cell products in medicine: Future of off-the-shelf products" in *Stem Cell Drugs - A New Generation of Biopharmaceuticals*, P. Van Pham, Ed. (Springer, Cham, Switzerland, 2018), pp. 93–118.
21. W. Katagiri, M. Osugi, T. Kawai, H. Hibi, First-in-human study and clinical case reports of the alveolar bone regeneration with the secretome from human mesenchymal stem cells. *Head Face Med.* **12**, 5 (2016).
22. W. Katagiri, M. Osugi, K. Kinoshita, H. Hibi, Conditioned medium from mesenchymal stem cells enhances early bone regeneration after maxillary sinus floor elevation in rabbits. *Implant Dent.* **24**, 657–663 (2015).
23. W. Katagiri *et al.*, A defined mix of cytokines mimics conditioned medium from cultures of bone marrow-derived mesenchymal stem cells and elicits bone regeneration. *Cell Prolif.* **50**, e12333 (2017).
24. D. Davidson *et al.*, Fibroblast growth factor (FGF) 18 signals through FGF receptor 3 to promote chondrogenesis. *J. Biol. Chem.* **280**, 20509–20515 (2005).
25. M. B. Ellman *et al.*, Fibroblast growth factor control of cartilage homeostasis. *J. Cell. Biochem.* **114**, 735–742 (2013).
26. E. E. Moore *et al.*, Fibroblast growth factor-18 stimulates chondrogenesis and cartilage repair in a rat model of injury-induced osteoarthritis. *Osteoarthritis Cartilage* **13**, 623–631 (2005).
27. H. E. Bergan-Roller, M. A. Sheridan, The growth hormone signaling system: Insights into coordinating the anabolic and catabolic actions of growth hormone. *Gen. Comp. Endocrinol.* **258**, 119–133 (2018).
28. C. Carter-Su, J. Schwartz, L. S. Argetsinger, Growth hormone signaling pathways. *Growth Horm. IGF Res.* **28**, 11–15 (2016).
29. J. Rui *et al.*, Controlled release of vascular endothelial growth factor using poly-lactic-co-glycolic acid microspheres: In vitro characterization and application in polycaprolactone fumarate nerve conduits. *Acta Biomater.* **8**, 511–518 (2012).
30. R. Dinarvand, S. H. Moghadam, A. Sheikhi, F. Atyabi, Effect of surfactant HLB and different formulation variables on the properties of poly-D,L-lactide microspheres of naltrexone prepared by double emulsion technique. *J. Microencapsul.* **22**, 139–151 (2005).
31. S. Adães *et al.*, Intra-articular injection of collagenase in the knee of rats as an alternative model to study nociception associated with osteoarthritis. *Arthritis Res. Ther.* **16**, R10 (2014).
32. W. J. O'Connor, T. Botti, S. N. Khan, J. M. Lane, The use of growth factors in cartilage repair. *Orthop. Clin. North Am.* **31**, 399–410 (2000).
33. M. Shakibaei, C. Seifarth, T. John, M. Rahmanzadeh, A. Mobasheri, Igf-I extends the chondrogenic potential of human articular chondrocytes in vitro: Molecular association between Sox9 and Erk1/2. *Biochem. Pharmacol.* **72**, 1382–1395 (2006).
34. W. Wang, D. Rigueur, K. M. Lyons, TGFβ signaling in cartilage development and maintenance. *Birth Defects Res. C Embryo Today* **102**, 37–51 (2014).
35. A. Jaklenec *et al.*, Sequential release of bioactive IGF-I and TGF-β 1 from PLGA microsphere-based scaffolds. *Biomaterials* **29**, 1518–1525 (2008).
36. P. Bora, A. S. Majumdar, Adipose tissue-derived stromal vascular fraction in regenerative medicine: A brief review on biology and translation. *Stem Cell Res. Ther.* **8**, 145 (2017).
37. Y. Chen *et al.*, Macrophages in osteoarthritis: Pathophysiology and therapeutics. *Am. J. Transl. Res.* **12**, 261–268 (2020).

38. H. Zhang, D. Cai, X. Bai, Macrophages regulate the progression of osteoarthritis. *Osteoarthritis Cartilage* **28**, 555–561 (2020).
39. B. Liu, M. Zhang, J. Zhao, M. Zheng, H. Yang, Imbalance of M1/M2 macrophages is linked to severity level of knee osteoarthritis. *Exp. Ther. Med.* **16**, 5009–5014 (2018).
40. M. Daheshia, J. Q. Yao, The interleukin 1β pathway in the pathogenesis of osteoarthritis. *J. Rheumatol.* **35**, 2306–2312 (2008).
41. H. Takaki *et al.*, TGF-β1 suppresses IFN-γ-induced NO production in macrophages by suppressing STAT1 activation and accelerating iNOS protein degradation. *Genes Cells* **11**, 871–882 (2006).
42. R. K. Studer, Nitric oxide decreases IGF-1 receptor function in vitro; glutathione depletion enhances this effect in vivo. *Osteoarthritis Cartilage* **12**, 863–869 (2004).
43. H. L. Reesink, A. E. Watts, H. O. Mohammed, G. D. Jay, A. J. Nixon, Lubricin/proteoglycan 4 increases in both experimental and naturally occurring equine osteoarthritis. *Osteoarthritis Cartilage* **25**, 128–137 (2017).
44. J. Desrochers, M. W. Amrein, J. R. Matyas, Microscale surface friction of articular cartilage in early osteoarthritis. *J. Mech. Behav. Biomed. Mater.* **25**, 11–22 (2013).
45. A. A. Young *et al.*, Proteoglycan 4 downregulation in a sheep meniscectomy model of early osteoarthritis. *Arthritis Res. Ther.* **8**, R41 (2006).
46. E. Teeple *et al.*, Coefficients of friction, lubricin, and cartilage damage in the anterior cruciate ligament-deficient guinea pig knee. *J. Orthop. Res.* **26**, 231–237 (2008).
47. K. A. Elsaid *et al.*, Decreased lubricin concentrations and markers of joint inflammation in the synovial fluid of patients with anterior cruciate ligament injury. *Arthritis Rheum.* **58**, 1707–1715 (2008).
48. K. A. Elsaid, J. T. Machan, K. Waller, B. C. Fleming, G. D. Jay, The impact of anterior cruciate ligament injury on lubricin metabolism and the effect of inhibiting tumor necrosis factor α on chondroprotection in an animal model. *Arthritis Rheum.* **60**, 2997–3006 (2009).
49. M. Bhattacharjee *et al.*, Preparation and characterization of amnion hydrogel and its synergistic effect with adipose derived stem cells towards IL1β activated chondrocytes. *Sci. Rep.* **10**, 18751 (2020).
50. Z. Sun, L. S. Nair, C. T. Laurencin, The paracrine effect of adipose-derived stem cells inhibits IL-1β-induced inflammation in chondrogenic cells through the Wnt/β-catenin signaling pathway. *Regen. Eng. Transl. Med.* **4**, 35–41 (2018).
51. M. B. Schmidt, E. H. Chen, S. E. Lynch, A review of the effects of insulin-like growth factor and platelet derived growth factor on in vivo cartilage healing and repair. *Osteoarthritis Cartilage* **14**, 403–412 (2006).
52. F. S. Loffredo *et al.*, Targeted delivery to cartilage is critical for in vivo efficacy of insulin-like growth factor 1 in a rat model of osteoarthritis. *Arthritis Rheumatol.* **66**, 1247–1255 (2014).
53. Z. Zhang *et al.*, The effects of different doses of IGF-1 on cartilage and subchondral bone during the repair of full-thickness articular cartilage defects in rabbits. *Osteoarthritis Cartilage* **25**, 309–320 (2017).
54. N. R. Danna *et al.*, The effect of growth hormone on chondral defect repair. *Cartilage* **9**, 63–70 (2018).
55. D. R. Kwon, G. Y. Park, Effect of intra-articular injection of AOD9604 with or without hyaluronic acid in rabbit osteoarthritis model. *Ann. Clin. Lab. Sci.* **45**, 426–432 (2015).
56. D. Reker *et al.*, Sprifermin (rhFGF18) versus vehicle induces a biphasic process of extracellular matrix remodeling in human knee OA articular cartilage ex vivo. *Sci. Rep.* **10**, 6011 (2020).
57. L. D. Solorio, E. L. Vieregge, C. D. Dhami, E. Alsberg, High-density cell systems incorporating polymer microspheres as microenvironmental regulators in engineered cartilage tissues. *Tissue Eng. Part B Rev.* **19**, 209–220 (2013).
58. J. C. Mora, R. Przkora, Y. Cruz-Almeida, Knee osteoarthritis: Pathophysiology and current treatment modalities. *J. Pain Res.* **11**, 2189–2196 (2018).
59. Z. Zhang, G. Huang, Intra-articular lornoxicam loaded PLGA microspheres: Enhanced therapeutic efficiency and decreased systemic toxicity in the treatment of osteoarthritis. *Drug Deliv.* **19**, 255–263 (2012).
60. J. Paik, S. T. Duggan, S. J. Keam, Triamcinolone acetonide extended-release: A review in osteoarthritis pain of the knee. *Drugs* **79**, 455–462 (2019).
61. J. Pradal *et al.*, Effect of particle size on the biodistribution of nano- and microparticles following intra-articular injection in mice. *Int. J. Pharm.* **498**, 119–129 (2016).
62. E. Horisawa *et al.*, Prolonged anti-inflammatory action of DL-lactide/glycolide copolymer nanospheres containing betamethasone sodium phosphate for an intra-articular delivery system in antigen-induced arthritic rabbit. *Pharm. Res.* **19**, 403–410 (2002).
63. E. Horisawa *et al.*, Size-dependency of DL-lactide/glycolide copolymer particulates for intra-articular delivery system on phagocytosis in rat synovium. *Pharm. Res.* **19**, 132–139 (2002).
64. B. Doyran *et al.*, Nanoindentation modulus of murine cartilage: A sensitive indicator of the initiation and progression of post-traumatic osteoarthritis. *Osteoarthritis Cartilage* **25**, 108–117 (2017).
65. A. E. Peters, R. Akhtar, E. J. Comerford, K. T. Bates, The effect of ageing and osteoarthritis on the mechanical properties of cartilage and bone in the human knee joint. *Sci. Rep.* **8**, 5931 (2018).